NeuroImage **14,** 298–309 (2001)
doi:10.1006/nimg.2001.0848, available online at http://www.idealibrary.com on IDEAL®

In Vivo Mapping of Gray Matter Loss with Voxel-Based Morphometry in Mild Alzheimer's Disease

J. C. Baron,*,†,[1] G. Chételat,* B. Desgranges,* G. Perchey,* B. Landeau,*
V. de la Sayette,*,‡ and F. Eustache*,‡

**INSERM U320 and ‡Department of Neurology, University of Caen, Caen, France; and †Department of Neurology, University of Cambridge, Cambridge, United Kingdom*

Received September 18, 2000

Up till now, the study of regional gray matter atrophy in Alzheimer's disease (AD) has been assessed with regions of interest, but this method is time-consuming, observer dependent, and poorly reproducible (especially in terms of cortical regions boundaries) and in addition is not suited to provide a comprehensive assessment of the brain. In this study, we have mapped gray matter density by means of voxel-based morphometry on T1-weighted MRI volume sets in 19 patients with mild AD and 16 healthy subjects of similar age and gender ratio and report highly significant clusters of gray matter loss with almost symmetrical distribution, affecting mainly and in decreasing order of significance the medial temporal structures, the posterior cingulate gyrus and adjacent precuneus, and the temporoparietal association and perisylvian neocortex, with only little atrophy in the frontal lobe. The findings are discussed in light of previous studies of gray matter atrophy in AD based either on postmortem or neuroimaging data and in relation to PET studies of resting glucose consumption. The limitations of the method are also discussed in some detail, especially with respect to the segmentation and spatial normalization procedures as they apply to pathological brains. Some potential applications of voxel-based morphometry in the study of AD are also mentioned.

INTRODUCTION

Postmortem studies in Alzheimer's disease (AD) have documented the presence of conspicuous cortical atrophy as a direct result of synaptic and neuronal loss (Masliah *et al.*, 1991; Double *et al.*, 1996; Bobinski *et al.*, 1996). Structural imaging with either CT or T1-weighted MRI allows brain atrophy to be assessed *in vivo*, and its added diagnostic value has been assessed especially in the early stages of the disease (for review, see Smith and Jobst, 1996; de Leon *et al.*, 1999). These studies have consistently reported that, in agreement with the well-established staging of tau neurofibrillary pathology distribution in AD (Braak and Braak; 1997; Delacourte *et al.*, 1999; Price and Morris, 1999), the first brain region to be affected by atrophy is the medial temporal lobe, which comprises the hippocampus proper, the parahippocampal gyrus (which itself includes the entorhinal and perirhinal cortices), and the amygdala (de Leon *et al.*, 1999; Bobinski *et al.*, 1999; Juottonen *et al.*, 1998; Lehéricy *et al.*, 1994; Frisoni *et al.*, 1999; Killiany *et al.*, 2000; Xu *et al.*, 2000). However, presumably because of the methods used (see below), very limited information is available about the status of other brain areas with respect of atrophy in AD.

Up till now, the study *in vivo* of regional brain atrophy in AD has almost exclusively relied on classic volumetry, which involves the summing of multiple region of interest (ROIs) drawn across a series of adjacent brain cuts. However, this method is time-consuming, observer dependent, and poorly reproducible, notably because of the uncertain relationships between cytoarchitectonic areas and surface landmarks as well as the complexity of regions such as the hippocampus–amygdala complex (Pruessner *et al.*, 2000; Hasboun *et al.*, 1996). Especially, the ROI method is not suited to allow a comprehensive assessment of the entire brain parenchyma, and as a result the number of brain regions that can be studied in any one investigation is limited. Because of these problems, a full account of the effects of AD on regional gray matter volumes for the entire brain is still lacking, and apart from the medial temporal structures, only scarce data about other brain areas are available, concerning only the lateral temporal and frontal cortices (Fama *et al.*, 1997; Bobinski *et al.*, 1999; Pantel *et al.*, 1997; Frisoni *et al.*, 1999; Erkinjutti *et al.*, 1993) and the anterior cingulate gyrus (Killiany *et al.*, 2000). Other methods to evaluate atro-

[1] To whom correspondence and reprint requests should be addressed at Department of Neurology, Box 165, Addenbrooke's Hospital, Cambridge, CB2 2QQ, UK. Fax: 44 1223 336941. E-mail: jcb54@cam.ac.uk.

1053-8119/01 $35.00

phy, such as linear (Frisoni *et al.,* 1996) and CSF space (de Leon *et al.,* 1999) measurements, do not directly assess volumes and therefore only provide rough indices of actual tissue loss.

Voxel-based methods using T1-weighted MRI have the potential to accomplish this goal. Although the method of Fox *et al.* (1996) allows quantitation of the loss of brain tissue in AD patients assessed longitudinally, it is not designed for direct statistical comparisons between groups and does not incorporate stereotaxic standardization. Voxel-based morphometry (VBM) on segmented MRI data volumes with spatial normalization has recently emerged as an ideal tool to map in an objective and comprehensive way the changes in gray matter density in disease states (Wright *et al.,* 1995; Ashburner and Friston, 1997, 2000). VBM has been extensively cross-validated with ROI measurements and functional correlates (Richardson *et al.,* 1997; May *et al.,* 1999; Maguire *et al.,* 2000) and has been used in correlation with neuropsychological scores in neurodegenerative disorders (Mummery *et al.,* 2000). A short paper describing findings with VBM in AD has been published recently (Rombouts *et al.,* 2000), but it assessed only small samples of patients and controls, which may expose to inadequate statistical power. In the present work, we applied VBM to the investigation of mild AD using substantial samples of both patients and controls. In this work, we used SPM99, which has been cleared of errors in the segmentation procedures present in earlier versions (Ashburner and Friston, 2000).

SUBJECTS AND METHODS

Subjects

We studied 19 patients (mean age 73 ± 5 years; range 63–85 years) with typical clinical presentation fulfilling NINCDS-ADRDA criteria for probable AD (McKhann *et al.,* 1984) of mild severity (MMS = 22.4 ± 2.5; range 17–26). The diagnosis of probable AD was based on an extensive neuropsychological examination which, apart from the MMS, included the Mattis dementia scale; Wechsler's memory scale, the Story and Figure recall tests from Signoret's battery, verbal span (forward and reverse), verbal working memory (Brown–Peterson paradigm), verbal fluency (letter and category), and copy of Rey's figure. We also studied 16 unmedicated healthy controls, aged 57 to 83 years (mean 66 ± 8 years, range 57–83 years), with normal memory performance and without vascular lesions at MRI. The two groups were matched for gender (11 women and 8 men in the AD group and 9 women and 7 men in the control group, respectively). The controls were screened for the absence of cerebrovascular risk factors, mental disorder, substance abuse, head trauma, significant MRI or biological abnormality, and incipient dementia using a memory test battery. To avoid head motion during scanning, all the patients studied here were fully cooperative and free from behavioral disturbances. Informed consent was obtained from all subjects.

MRI

For each subject, a high-resolution T1-weighted volume MRI scan was obtained, which consisted of a set of 128 adjacent axial cuts parallel to the AC–PC line and with slice thickness 1.5 mm and pixel size 1 × 1 mm, using the SPGR gradient echo sequence (TR = 15.4 s; TE = 3.4 kHz; FOV = 24 × 24; matrix = 256 × 256). All the MRI data sets were acquired on the same scanner (1.5-T Signa Advantage echospeed; General Electric) and with the same parameters. Standard correction for field inhomogeneities was applied at acquisition.

Image Handling and Transformations

Using SPM99 (Wellcome Department of Cognitive Neurology, London, UK), the raw MRI sets were segmented into four tissue classes (gray, white, CSF, and other). The segmentation procedure involves calculating for each voxel a Bayesian probability of belonging to each tissue class based on *a priori* MRI information (Ashburner and Friston, 1997, 2000). To allow this, an approximate (12-parameter affine only) and reversible spatial normalization of the MRI sets was performed before segmentation, using the standard T1-MR set of SPM99, which is based on the 305 normal data set of Montreal Neurological Institute; a nonuniformity correction was included, as prescribed (Ashburner and Friston, 2000). The segmented gray matter sets were then subjected to an affine and nonlinear spatial normalization into standard Talairach and Tournoux (1988) space, using the standard gray matter template of SPM99, with medium regularization and a reslicing of 2 × 2 × 2 mm. Masking was not used in this normalization process. The spatially normalized set was then smoothed with a 12-mm full width at half-maximum Gaussian filter to reduce confounding by individual variation in gyral anatomy and to increase the signal-to-noise ratio (Mummery *et al.,* 2000). The method is illustrated in Fig. 1.

Statistical Analysis

The data (without normalization for the total amount of gray matter) of the two groups of subjects were then compared statistically (using the $T > 3.36$ cutoff, which corresponds to $P < 0.001$), based on the general linear model and random Gaussian field theory (Friston *et al.,* 1995a,b); the "compare populations; one scan per subject, two-sample *t* test" routine was used. The degrees of freedom were 33 from 35 images. The threshold used for selection of voxels was 40% of grand mean value. The total number of voxels analyzed was

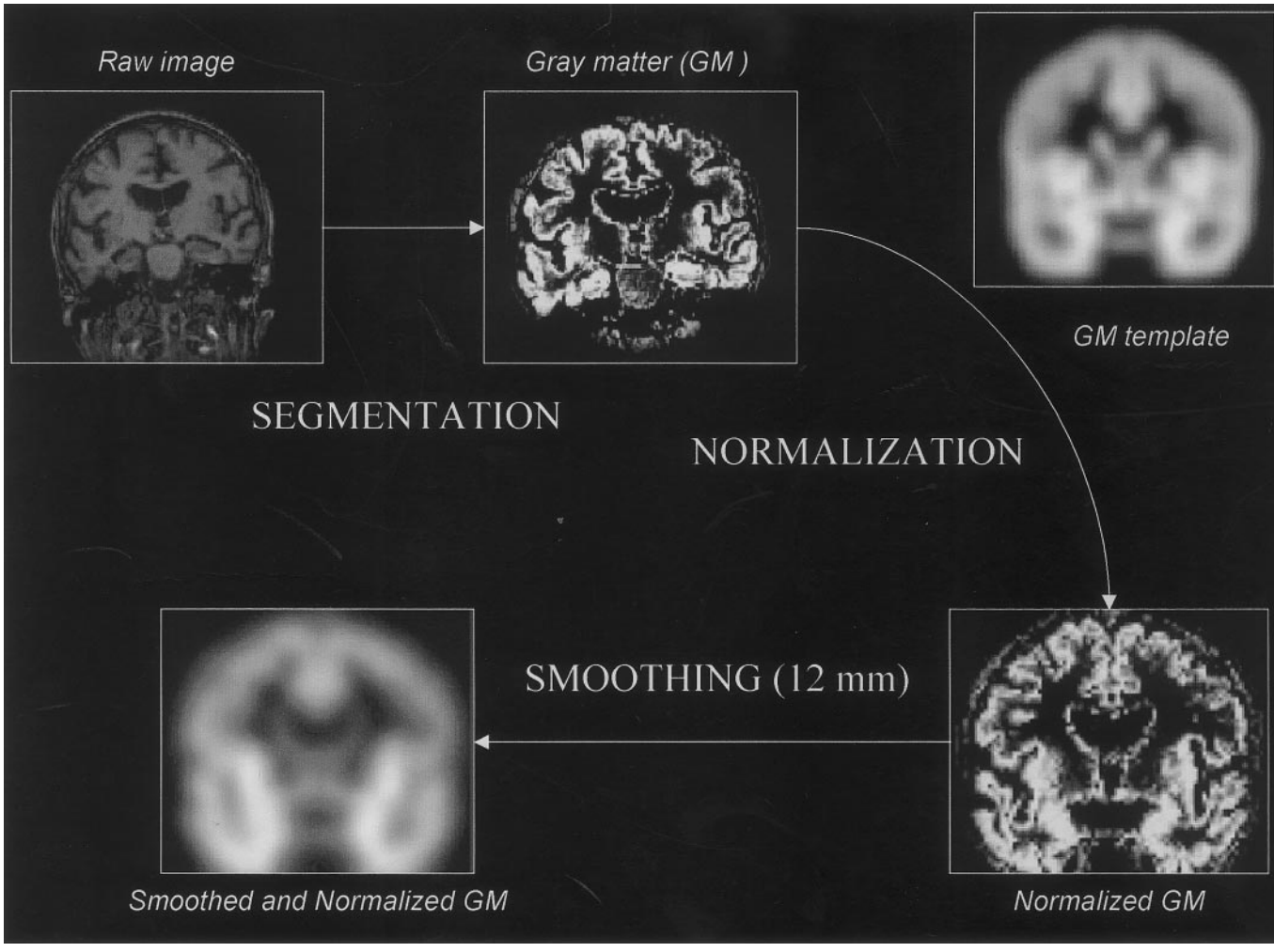

FIG. 1. The three steps used for image analysis of the raw MR data set, namely, segmentation, normalization, and smoothing, illustrated here for a typical Alzheimer's disease patient data set and for a coronal brain slice passing through the hippocampal region (note the substantial degree of bilateral hippocampal atrophy as well as dilatation of the sylvian fissure present in this case). Although not illustrated in this figure, the segmentation routine included an approximate (affine only) and reversible spatial normalization that used the standard T1-MR set of SPM99 and was meant to allow the attribution to each voxel of a probability to belong to each tissue class based on *a priori* images (see Subjects and Methods).

221,432. To limit the number of statistical tests and the attending risk of false positives, only reductions in gray matter density in AD patients relative to controls were assessed, and only clusters with $P < 0.10$ corrected for multiple comparisons were considered significant (for this correction, we used the standard method based on 3D Gaussian fields of Friston *et al.*, 1995b; and Worsley *et al.*, 1996; and implemented in SPM99). Anatomical localization was according to Talairach's atlas, using M. Brett's set of linear transformations (see www.mrc-cbu.cam.ac.uk/Imaging/mnispace.html).

The above analysis was repeated but this time using the Proportional Scaling routine, which normalizes the gray matter sets across subjects to overall grand mean. This ancillary analysis was meant to assess the relative distribution of gray matter atrophy in AD compared to controls. Thus, only decreases in relative gray matter density were assessed. To account for the expected loss of sensitivity compared to the above analysis, the more liberal $P < 0.001$ (uncorrected) cutoff was used.

RESULTS

The results for the main analysis are summarized in Table 1 and illustrated in Figs. 2 and 3. Briefly, significant clusters of reduced gray matter density were found to affect in an essentially symmetrical way and in approximate decreasing order of statistical significance, the amygdala/anterior hippocampus/entorhinal cortex areas, posterior cingulate cortex and adjacent precuneus, perisylvian areas, temporoparietal association neocortex (with left-sided predominance), posterior hippocampus, anterior hypothalamus and thalamus, prefrontal cortex (also with left-sided predominance), and caudate nucleus and putamen. The comparison of the total amount of gray matter between the two groups revealed a significant reduction in the

TABLE 1

SPM99 Results from the Analysis of Decreases in Gray Matter Density in 19 Patients with Probable Alzheimer's Disease Relative to 16 Age-Matched Healthy Controls, Using as Cutoff the $P < 0.10$ Cluster Level Corrected for Multiple Tests

P (corrected)	k	Region	Coordinates (mm)			Z
			x	y	z	
0.000	9686	R amygdala/entorhinal cortex/hippocampus	20	−4	−12	4.95
		R sylvian fissure/insula	44	−14	−3	4.74
		L amygdala/entorhinal cortex/hippocampus	−24	−8	−13	4.65
		L amygdala	−24	−5	−17	4.64
		R mid. temporal gyrus	51	−22	−6	4.57
		L sylvian fissure	−48	−30	20	4.53
		R post.-hippocampus	32	−33	−2	4.49
		L inf. parietal lobule	−50	−15	17	4.42
		L ant. hypothalamus	−4	4	−7	4.26
		Third ventricle	2	−2	−2	4.20
		R ant. hypothalamus	4	2	−7	4.19
		Third ventricle	2	−2	−7	4.17
		R sup. temporal gyrus	55	4	−5	4.15
		L mid. temporal gyrus	−63	−46	4	4.13
		L caudate nucleus (head)	−6	2	5	4.09
		L sup. temporal gyrus	−53	2	−8	4.07
		L ant. thalamus	−2	−16	1	4.05
		R sup. temporal gyrus	61	−46	15	4.02
		L sylvian fissure/insula	−38	−10	0	3.93
		R sup. temporal gyrus	57	−55	19	3.92
		L mid. temporal gyrus	−59	−35	0	3.91
		L mid. temporal gyrus	−59	−24	−4	3.79
		R sylvian fissure/insula	42	−3	9	3.77
		L sup. temporal gyrus	−61	−16	1	3.64
		R. inf. frontal gyrus	44	21	1	3.62
		R inf. parietal lobule	51	−22	18	3.61
		L ant. putamen	−24	10	−2	3.58
		R sylvian fissure/insula	36	20	3	3.54
		R inf. parietal lobule	44	−15	17	3.52
		L sup. temporal gyrus	−46	−17	6	3.45
		R inf. parietal lobule	53	−32	26	3.38
		R inf. temporal gyrus	57	−66	3	3.33
		R mid. temporal gyrus	59	−62	1	3.29
		L sup. temporal gyrus	−63	−40	13	3.23
		R inf. parietal lobule	55	−41	28	3.17
		R caudate nucleus (head)	8	2	11	3.15
		R sylvian fissure/insula	36	17	−6	3.10
0.000	1154	R post. cingulate gyrus/precuneus	10	−35	37	4.75
		L post. cingulate gyrus/precuneus	−10	−35	40	4.33
		R/L post. cingulate gyrus	0	−10	30	3.44
		R/L post. cingulate gyrus	0	−18	34	3.43
0.025	331	L inf. parietal lobule (SMG)	−44	−52	49	4.18
		L inf. parietal lobule (SMG)	−51	−47	41	3.64
0.089	219	L post. hippocampus	−30	−37	−2	3.72
		L post. hippocampus	−30	−47	−1	3.62
0.090	218	L angular gyrus	−48	−71	22	3.69
		L angular gyrus	−51	−57	29	3.43
0.050	268	L mid. frontal gyrus	−48	30	24	3.69
		L mid. frontal gyrus	−48	21	23	3.61
		L inf. frontal gyrus	−46	7	25	3.59

Note. Results are listed by clusters and in decreasing order of peak Z score value. Cluster size is indicated by the value k, which represents the number of significant ($Z > 3.09$) voxels in the particular cluster. Talairach coordinates were obtained as explained under Subjects and Methods. L, left; R, right; ant., anterior; post., posterior; mid., middle; sup., superior; inf., inferior; SMG, supramarginal gyrus.

AD compared to the control group (0.344 ± 0.021 vs 0.365 ± 0.013, respectively; $P = 0.0012$). For the sake of curiosity, the reverse contrast (i.e., reductions in gray matter density in controls relative to patients) was also run, which yielded no significant cluster.

The results for the ancillary analysis are shown in Table 2 and Fig. 4. Briefly, the findings were almost identical to those from the main analysis, except that the extent of the clusters and the Z score of the peak voxels were considerably reduced, as expected. The

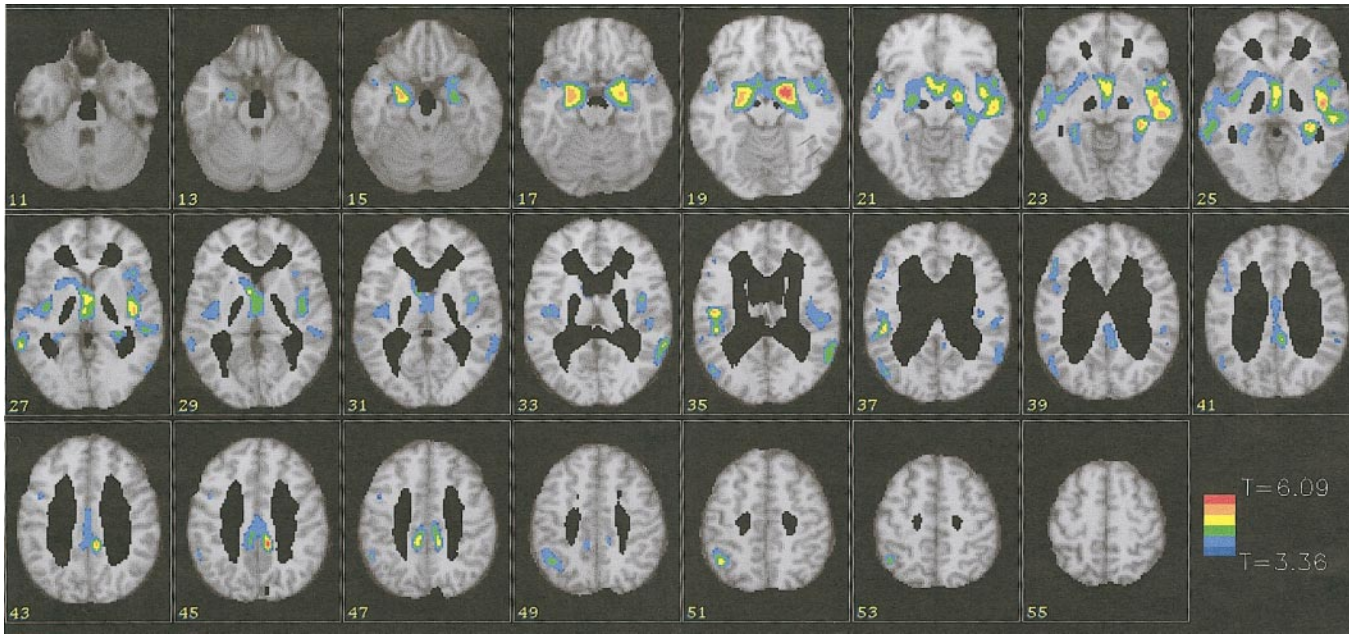

FIG. 2. Display showing the voxels with significantly reduced gray matter density in the group of 19 Alzheimer's disease patients compared to the group of 16 healthy age-matched controls, obtained using SPM99 and the $P < 0.10$ (cluster level, corrected for multiple tests) cut off (see Subjects and Methods). The significant voxels ($T > 3.36$) have been projected onto a normal MRI set spatially normalized to Talairach's template, but where only the analyzed voxels (i.e., above 40% of the mean whole brain value) are displayed. The right hemisphere corresponds to the right side of the figure; the axial reference plane, i.e., 0 mm relative to the bicommissural plane, is cut 25 above, with the other cuts every 4 mm above or below this plane. The voxels are displayed according to the pseudo-color T scale shown on the bottom right-hand corner.

only area revealed by this ancillary analysis but not by the main analysis was the anterior cingulate gyrus; however, exactly the same area was in fact also listed in the SPM printout for the main analysis, but it lay just below the stringent cutoff used (cluster-level corrected $P = 0.102$; $Z = 3.99$; $x = 4$, $y = 34$, $z = 10$). In addition to the findings for the ancillary analysis, and to illustrate this striking similarity between the two analyses, Fig. 4 also illustrates using the same presentation the results for the main analysis as well as those from the ancillary analysis but using a lower threshold ($P < 0.01$, uncorrected).

DISCUSSION

This study provides the first full and detailed account of gray matter atrophy in early Alzheimer's disease. On the background of a significant global atrophy, one important finding is the overall striking symmetry of the effects, with however the posterior parietal cortex (angular gyrus) and the dorsal frontal cortex showing preferentially left-sided atrophy (see Fig. 2). The data also reveal a striking limbic/paralimbic systems predominance of effects, notably affecting the anterior hippocampus, amygdala, entorhinal cortex, and posterior cingulate cortex (PCC), with a number of association cortical areas and some gray matter nuclei being also, though less prominently, affected. Another clear feature of our findings is the predominance of effects on the medial and posterior structures of the brain relative to the frontal lobes. Finally, there was a remarkable sparing of the primary cortices—either motor or sensory—of the inferior occipitotemporal regions as well as of the cerebellum, all regions known to have little or no cellular pathology until advanced stages of the disease (Braak and Braak, 1997; Larner, 1997). The analysis of the relative distribution of gray matter loss using the Proportional Scaling routine did not reveal important additional findings.

Before discussing these findings, three methodological issues merit consideration. First, although the difference in mean age between the AD and control groups was only 7 years, it was statistically significant and thus the question arises whether this may have confounded some of the findings with VBM, inasmuch as normal aging is known to also entail some degree of brain atrophy. Imperfect age matching may occur when as here the emphasis is on healthy—as opposed to standard—aging, substantially constraining the recruitment of healthy aged subjects. In the only other report on VBM in AD, the controls subjects were also on average 7 years younger than the patients (Rombouts *et al.*, 2000). To assess whether age influenced our findings, we reanalyzed our data in two ways: (i) by including a confound of age in the design matrix of the original groups and (ii) by constructing a smaller but perfectly age-matched subsample of control subjects

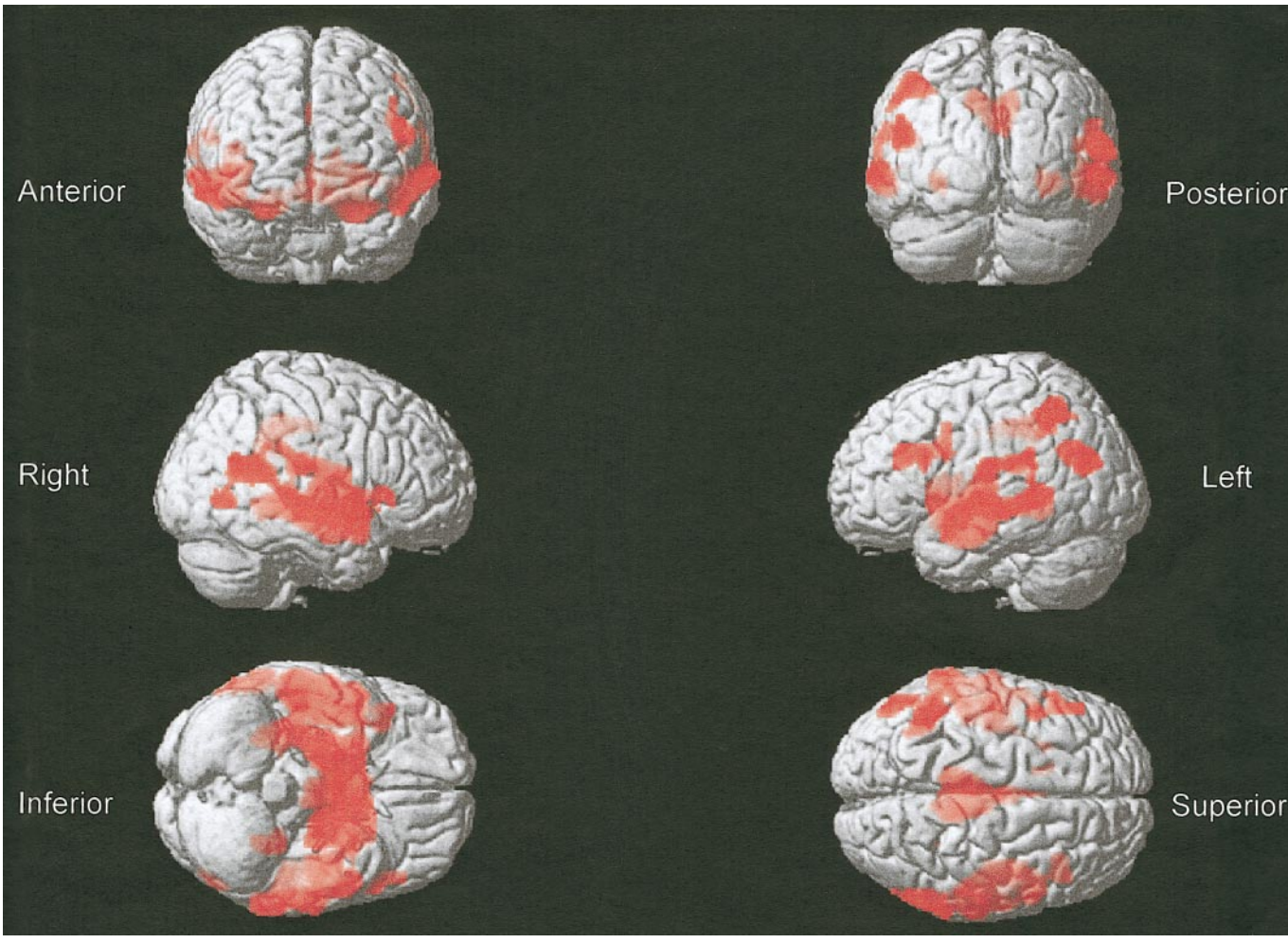

FIG. 3. SPM99 surface rendering depicting in red the significant ($P < 0.10$, corrected for multiple comparisons) clusters of voxels with gray matter density decreases (T score > 3.36) in 19 Alzheimer's disease patients compared to 16 age-matched controls, projected on a standard T1-weighted MRI for anatomical orientation, according to the six views indicated on the side of each image (see Subjects and Methods and Results). Although the data shown here are the same as those shown in Fig. 1, the surface rendering allows a better grasp of the actual topography of the atrophic changes than two-dimensional axial cuts (note for instance the atrophy of the posterior cingulate–precuneus areas, which bears a striking resemblance to the pattern of glucose hypometabolism reported in early AD, see for instance Minoshima *et al.*, 1997).

($n = 10$; mean age 71 years, range 61–83 years). The results from these two analyses were strikingly similar both to one another and to the original analysis, recovering all the main regions found with the latter, the only substantial difference being an inversion in the order of significance between lateral temporal/perisylvian and medial temporal regions. However, both approaches resulted in lower statistical significance of the findings, in part attributable to a reduction in the degrees of freedom and exposing to the risk of false negatives. The findings with the SPM analysis taking age as a confound are tabulated in Appendix 1. This table lists the clusters with corrected $P < 0.10$ as for the original analysis, as well as the five peak voxels with $Z > 3.75$ from the clusters that did not pass this stringent criterion, so as to account for the loss of statistical power. As can be seen, the main regions identified in the original analysis were recovered, especially the lateral temporal/insula/perisylvian region bilaterally, amygdala/hippocampus/entorhinal region bilaterally, right posterior hippocampus, left caudate head/bilateral hypothalamic/third ventricle area, left inferior parietal lobule, and right posterior cingulate cortex (the left PCC was significant but at a lower Z score of 3.43). Overall, therefore, the main findings from the original analysis do not appear to be due to the small age difference between the two subject groups.

Second, the VBM method as implemented in SPM99 is not without limitations and potential problems (see Ashburner and Friston, 2000, for a detailed discussion). One issue relates to the spatial normalization procedure to apply before segmentation in SPM99 (see discussions in SPM internet forum). In this work, we elected to segment the images based on a mild, affine only, and reversible normalization and to apply the full

TABLE 2

SPM99 Results from the Analysis of Decreases in Normalized Gray Matter Density in 19 Patients with Probable Alzheimer's Disease Relative to 16 Age-Matched Healthy Controls, Using the Proportional Scaling Routine with a Cutoff the $P < 0.001$, Uncorrected for Multiple Tests

P (corrected)	k	Region	Coordinates (mm) x	y	z	Z
0.021	290	R sylvian fissure/insula	46	−14	−1	4.36
		R mid. temporal gyrus	51	−20	−6	3.78
		R sup. temporal gyrus	44	−2	−10	3.25
0.864	49	R post. cingulate gyrus/precuneus	10	−37	37	3.99
0.004	407	R amygdala/entorhinal cortex hippocampus	14	−3	−12	3.96
		Third ventricle	2	−4	0	3.66
		R ant. hypothalamus	4	−2	−8	3.55
		L ant. thalamus	−2	−14	1	3.47
		L caudate nucleus (head)	−8	4	7	3.57
0.481	95	R post.-hippocampus	34	−35	−2	3.75
0.999	12	L sylvian fissure	−48	−32	20	3.62
0.986	24	L inf. parietal lobule (SMG)	−42	−52	47	3.47
1.000	1	R ant. cingulate gyrus	4	32	9	3.10
1.000	1	L amygdala/entorhinal cortex/hippocampus	−16	−3	−13	3.10

Note. Results are listed by clusters and in decreasing order of peak Z score value. Cluster size is indicated by the value k, which represents the number of significant voxels in the particular cluster. Talairach coordinates were obtained as explained under Subjects and Methods. L, left; R, right; ant., anterior; post., posterior; mid., middle; sup., superior; inf., inferior; SMG, supramarginal gyrus.

spatial normalization process (i.e., with both affine transform and nonlinear warping) only onto the segmented gray matter set and then based on the standard gray matter template. Presumably because of segmentation errors due to partial volume effects inherently created by warping, the use of standard full normalization prior to segmentation appears to increase the risk of misclassification of nonbrain tissue as gray matter voxels. As illustrated in Fig. 1 for an AD brain, our segmentation procedure did efficiently classify gray matter regions, inclusive of the atrophic hippocampal region, but evidently resulted also in some scalp, diploic space, and sagittal sinus misclassified voxels, indicating that it was not immune to this kind of problem. Although the addition of an automated brain extraction step can in principle address this problem, not only would this add to an already time-consuming procedure, but also would expose the risk of eroding the brain surface and therefore of missing authentic gray matter voxels in the final analysis. To control for this, most brain extraction routines, even if automated, include a provision for manual editing, which however has inherent potential observer bias. Even though we did not implement this additional step in our study, the misclassified voxels were eventually excluded from the statistical analyses in SPM because

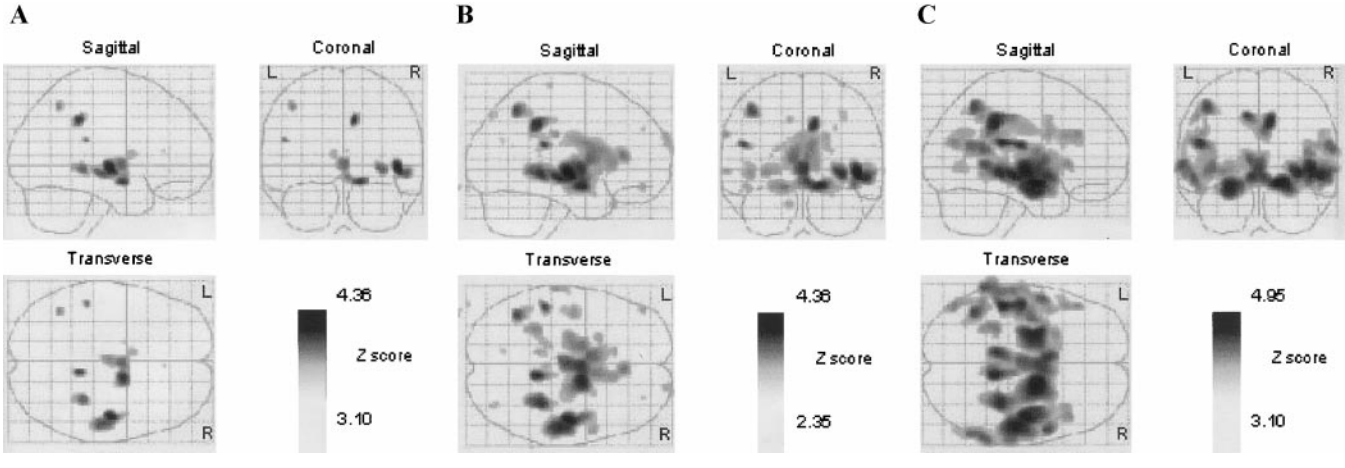

FIG. 4. "Glass brain" representations of the results from the Proportional Scaling analysis at the $P < 0.001$ (A) and $P < 0.01$ (B) cutoffs, and from the main analysis (C), illustrating that the findings were almost identical among all three analyses, the only difference being the expected lower sensitivity with the Proportional Scaling analysis (see Subjects and Methods and Results for details and Tables 1 and 2 for the actual lists of SPM peaks).

they exhibited a low probability of belonging to gray matter (see Fig. 1) and thus were excluded as part of the routine thresholding to 40% of grand mean (see Subjects and Methods). This is clearly illustrated in Fig. 2, which shows that, except for a few diploic space voxels in the upper transverse cuts, virtually no nonbrain voxels were included in the final statistical analysis. For the sake of comparison between our approach and the classical one, we also performed *post hoc* the analysis with full spatial normalization prior to segmentation (using the standard T1-weighted MR template of SPM99), and the results using the same statistical threshold are shown in Appendix 2. Overall, the results are very similar to those obtained in our method, but with three caveats: first, there was a large cluster extending beyond the brain boundaries in the vicinity of the right parietal lobe, a problem not encountered with the original method; second, the significant changes were not as symmetrically arranged as with the original method; and finally, the medial temporal region was not the most significantly affected, contrary to what would be expected based on previous ROI-based literature (see discussion below). Another issue relates to the use in pathologic populations of standard templates from young healthy male subjects for both the a priori images and the spatial normalization. Although a gray matter template specifically constructed for Alzheimer's disease could be constructed, the 305 MRI sets SPM99 templates offer considerable robustness, which may offset the lack of disease specificity. Finally, the patients studied here were all in the early stage of the disease where no major brain distortion is expected, and visual inspection suggested that the AD brains normalized reasonably well to the SPM template. Nevertheless, future studies should address this issue in a formal and systematic way.

Third and finally, VBM does not have the anatomical precision attainable by classic ROI-based volumetric studies. This is because of the need to spatially normalize and smooth the data in order to reduce the effect of intersubject differences in normal gyral anatomy and in turn to allow for a statistical, voxelwise analysis across subjects. It is thus difficult from the present data to describe the anatomical structures affected by atrophy with the precision afforded by single-subject volumetry, for instance, among the different parts of the rhinal cortex or within the hippocampus itself. However, this limitation should not detract from the considerable advantages of the voxel-based analysis in terms of efficiency, comprehensiveness, and freedom from observer bias.

The fact that the atrophy predominated in the medial temporal regions is entirely consistent with both ROI-based studies of mild-to-moderate AD (see de Leon *et al.*, 1999; Smith and Jobst, 1996; for review) and histopathological evidence that the hippocampal and rhinal cortices are the earliest affected by tau neurofibrillary pathology in AD over and above that present in normal aging (Braak and Braak, 1997; Delacourte *et al.*, 1999; Price and Morris, 1999; Haratounian *et al.*, 1999; Duyckaerts *et al.*, 1998). In the VBM study of Rombouts *et al.* (2000), the maximal degree of atrophy was found in the middle temporal gyrus, followed by the hippocampus, but in this study the segmentation was done on spatially normalized data sets. Atrophy of the amygdala was particularly prominent in our study, consistent with the fact that this medial temporal structure is also a major focus of pathology in AD and is among the most affected by tissue loss in ROI-based MRI studies (Maunoury *et al.*, 1996). The voxel-based relationships between the degree of atrophy of these medial temporal structures and neuropsychological impairment, especially with respect to episodic memory (Lehéricy *et al.*, 1994; Fama *et al.*, 1997), will be the topic of a separate report.

Our study documents a striking bilateral atrophy of the PCC and neighboring precuneus. To the best of our knowledge, *in vivo* measures of atrophy of this region in AD have never been reported. However, neuronal loss and neurofibrillary tangles have been found in the PCC postmortem, and cell damage in this area apparently develops soon after the medial temporal structures (Braak and Braak, 1997; Delacourte *et al.*, 1999; Vogt *et al.*, 1998). Based on functional imaging data in healthy subjects (see Desgranges *et al.*, 1998a, for review) and amnesia, inclusive of AD (Eustache *et al.*, 2000, for review), atrophy of this region in mild AD may have important implications in terms of memory dysfunction. The topography of atrophy of the PCC and precuneus area revealed by our study and illustrated by the surface rendering shown in Fig. 2 is strikingly similar to that reported in PET studies of resting glucose consumption in early AD (Minoshima *et al.*, 1997; Reiman *et al.*, 1996; Small *et al.*, 2000), suggesting that early atrophy may at least in part account for these PET observations and calling for a reassessment of the role of focal atrophy in physiologic imaging. The lack of significant atrophy of the anterior cingulate cortex in this study is consistent with the ROI study of Killiany *et al.* (2000).

Atrophy in the sylvian fissure/insular region is consistent with both the dilatation of the sylvian fissure known to develop over time in AD and the recent VBM study of Rombouts *et al.* (2000). Atrophy of insular and perisylvian cortex at postmortem has been reported by Price and Morris (1999) and Van Hoesen *et al.* (2000) and *in vivo* by Foundas *et al.* (1997) (see also Fig. 1 for an illustration of this). In the present work, we did not attempt to correlate gray matter density with disease duration because of the well-known uncertainty in estimating the latter in AD.

Previous ROI-based studies have suggested that temporal neocortical areas are affected by atrophy immediately after the medial temporal areas (de Leon *et al.*, 1999; Killiany *et al.*, 2000; Erkinjutti *et al.*, 1993), in agreement with the histopathological staging of AD

(Braak and Braak, 1997; Delacourte *et al.*, 1999). Our findings concur with this, although as noted above, atrophy of the PCC and sylvian/insular cortex appeared more prominent. Longitudinal studies would be helpful to establish the exact distribution of atrophy progression in AD.

ROI-based studies have rarely assessed the inferior parietal lobule and angular gyrus in AD (Foundas *et al.*, 1997). Our finding that these areas are among the most affected in AD are however consistent with histopathological studies showing substantial cellular pathology in these areas in AD (Haratounian *et al.*, 1999; Delacourte *et al.*, 1999; Grignon *et al.*, 1998). A left-sided predominance of atrophy of the angular gyrus in our study would be consistent with some early PET reports (Lowenstein *et al.*, 1989).

Our findings suggesting gray matter loss in the vicinity of the anterior hypothalamus, third ventricle, and anterior thalamus are consistent with the notion that the third ventricle is significantly dilated in AD (Fama *et al.*, 1997). Likewise, atrophy of the caudate head has not been reported with ROI-based studies previously, but is consistent with the findings of Rombouts *et al.* (2000) using VBM in a limited set of patients. We also report here a mildly significant atrophy of the anterior putamen, heretofore undescribed.

Finally, our data document some degree of atrophy in frontal regions (especially around Brodmann's area 47 on the right and Broca's area on the left), with a clear predominance over the left hemisphere. Earlier MRI studies have also reported some degree of frontal lobe atrophy in AD, but to such a mild degree as to have no clear diagnostic value (Fama *et al.*, 1997; Frisoni *et al.*, 1996; Pantel *et al.*, 1997). Regarding postmortem data, neuronal loss, synaptic loss, and tau pathology have been repeatedly reported to occur in frontal regions in AD (Double *et al.*, 1996; Price and Morris, 1999; Van Hoesen *et al.*, 2000; Masliah *et al.*, 1991; Haratounian *et al.*, 1999).

Although obviously speculative at this stage, it will be of interest to see whether VBM is of any value in assessing the individual atrophy pattern in AD especially for diagnostic applications at the early stages of the disease and in following on a voxel-by-voxel basis the time-course of atrophy; VBM might also serve as a surrogate marker in assessing the effects of agents designed to slow or interrupt the disease process, compared to the natural course of atrophy. Finally, VBM may help identify in a voxel-based way the brain regions whose pathology underlies the cognitive impairment in AD and provide a template upon which to allow voxel-based atrophy correction of functional imaging data (Ibanez *et al.*, 1997).

ACKNOWLEDGMENTS

The authors are indebted to M-H. Noel, M-C. Onfroy, and D. Luet for their help in the MRI scanning, image transfer, and handling and to B. David for her help with the illustrations for this paper.

APPENDIX 1

Same Analysis as in Table 1, but with Age Being Covaried for in the Comparison

P (corrected)	*k*	Region	Coordinates (mm) *x*	*y*	*z*	*Z*
0.000	1322	R mid. temporal gyrus	55	5	−9	4.27
		R insula	46	−24	−9	4.17
		R insula	44	−14	−3	4.01
		R post. hippocampus	34	−33	−3	3.97
		R insula	38	−4	−5	3.73
0.000	659	R amygdala/entorhinal cortex/hippocampus	20	−4	−12	4.07
		Third ventricle	0	−4	−1	3.46
		L caudate nucleus (head)	−6	2	5	3.33
		R ant. hypothalamus	6	0	−8	3.32
		L ant. hypothalamus	−4	4	−7	3.26
0.012	351	L amygdala/entorhinal cortex/hippocampus	−26	−3	−17	4.01
0.017	327	L mid. temporal gyrus	−53	−22	−9	3.71
		L mid. temporal gyrus	−57	−33	−2	3.66
		L mid. temporal gyrus	−63	−43	2	3.66
		L mid. temporal gyrus	−63	−39	0	3.59
0.169	*168*	*L sup. temporal gyrus*	*−57*	*0*	*−5*	*4.46*
0.345	*122*	*L inf. parietal lobule (SMG)*	*−50*	*−17*	*19*	*4.13*
0.350	*121*	*R mid. temporal gyrus*	*71*	*−43*	*−3*	*3.92*
0.750	*65*	*R post. cingulate gyrus/precuneus*	*10*	*−35*	*37*	*3.88*
0.790	*60*	*L fusiform gyrus*	*−65*	*−21*	*−23*	*3.90*

Note. As in Table 1, we used the $P < 0.10$ cluster-level corrected for multiple tests as cutoff, but we also list in italics the voxels with $Z > 3.75$ ($N = 5$) from clusters not reaching this stringent criterion (see Discussion). Layout and abbreviations as in Table 1.

APPENDIX 2

SPM99 Results for the Analysis of Decreases in Gray Matter Density in 19 Patients with Probable Alzheimer's Disease Relative to 16 Age-Matched Healthy Controls, with Full Spatial Normalization Being Done before Segmentation

P (corrected)	*k*	Region	Coordinates (mm)			*Z*
			x	*y*	*z*	
0.000	6783	L sup. temporal gyrus/sylvian fissure	−44	−14	1	4.85
		L mid. Temporal gyrus	−53	5	−10	4.77
		L sup. temporal gyrus	−51	7	−14	4.70
		L sup. temporal gyrus	−55	4	−7	4.67
		L sup. temporal gyrus	−46	−30	16	4.37
		L hypothalamus	−10	−2	−10	4.24
		Third ventricle	0	−4	−1	4.19
		L rolandic operculum	−48	−1	13	4.07
		Third ventricle	−2	−19	3	4.06
		R ant. Thalamus	4	−12	2	3.93
		L caudate (head)	−8	9	−7	3.88
		L caudate (head)	−8	10	5	3.86
		L mid. Temporal gyrus	−55	−12	−6	3.84
		L mid. Temporal gyrus	−57	−16	−4	3.83
		L mid. Temporal gyrus	−59	−10	−8	3.82
		L medial thalamus	−6	−23	9	3.80
		L medial thalamus	−8	−27	11	3.75
		L amygdala/entorhinal cortex/hippocampus	−28	−3	−17	3.68
		L ant. Putamen	−22	12	−2	3.66
		L post. hippocampus	−24	−39	4	3.65
		L post. thalamus	−12	−35	9	3.55
		L sup. temporal gyrus	−50	6	5	3.48
		L post.-central gyrus	−55	15	25	3.46
		L post.-central gyrus	−65	−14	25	3.30
		L caudate (head)	−14	5	15	3.25
0.000	2418	R inf. parietal lobule*	63	−38	26	4.71
		R inf. Parietal lobule	44	−50	50	4.32
		R inf. parietal lobule	53	−45	32	4.21
		R mid. Temporal gyrus*	67	−31	2	4.17
		R inf. parietal lobule	57	−41	35	4.17
		R mid. Temporal gyrus*	67	−43	4	4.06
		R sup. Parietal lobule	36	−64	49	4.04
		R sup. temporal gyrus*	67	−36	15	4.02
		R sup. temporal gyrus	53	−55	30	4.00
		R inf. parietal lobule	48	−40	50	3.95
		R inf. parietal lobule*	61	−27	44	3.90
		R sup. Parietal lobule	32	−72	46	3.74
		R post.-central gyrus	63	−20	30	3.62
		R mid. Temporal gyrus	50	−69	22	3.32
		R sup. Parietal lobule	32	−48	50	3.21
		R sup. temporal gyrus	51	−25	0	3.20
0.000	1529	R sylvian fissure/insula	42	−6	−1	4.60
		R amygdala/entorhinal cortex/hippocampus	26	−8	−11	4.18
		R. amygdala/entorhinal cortex/hippocampus	26	−5	−13	4.05
		R sup. temporal gyrus	42	9	−14	3.88
		R sup. temporal gyrus	44	9	−11	3.87
		R hippocampal fissure	18	−14	−8	3.82
		R hippocampal fissure	16	−18	−8	3.79
		R sup. temporal gyrus	53	9	−7	3.49
0.047	286	L precuneus/post. cingulate gyrus	−12	−42	43	4.21
		L post. cingulate gyrus	−11	−26	38	4.08
		L precuneus/post. cingulate gyrus	−12	−53	38	3.48

Note. The cutoff used was $P < 0.10$ cluster level, corrected for multiple tests. Layout and abbreviations as in Table 1, except that here an asterisk indicates coordinates falling outside the brain template boundaries.

REFERENCES

Ashburner, J., and Friston, K. 1997. Multimodal image coregistration and partitioning: A unified framework. *NeuroImage* **6:** 209–217.

Ashburner, J., and Friston, K. 2000. Voxel-based morphometry: The methods. *NeuroImage* **11:** 805–821.

Bobinski, M., Wegiel, J., Wisniewski, H. M., Taérnawski, M., Bobinski, M., Reisberg, B., de Leon, M., and Miller, D. C. 1996. Neurofibrillary pathology: Correlation with hippocampal formation atrophy in Alzheimer's disease. *Neurobiol. Aging* **17:** 909–919.

Bobinski, M., de Leon, M., Convit, A., de Santi, S., Wegiel, J., Tarshish, C. Y., Saint-Louis, L. A., and Wisniewski, H. M. 1999. MRI of entorhinal cortex in mild Alzheimer's disease. *Lancet* **353:** 38–40.

Braak, H., and Braak, E. 1997. Pattern of cortical lesions in Alzheimer's disease. In *Alzheimer's Disease: Biology, Diagnosis, and Therapeutics* (K. Iqbal, B. Winblad, T. Nishimura, M. Takeda, and H. M. Wisniewski, Eds.), pp. 227–237. Wiley, New York.

Delacourte, A., David, J. P., Sergeant, N., Buée, L., Waltez, A., and Vermersch, P., *et al.* 1999. The biochemical pathways of neurofibrillary degeneration in aging and Alzheimer's disease. *Neurology* **52:** 1158–1165.

De Leon, M. J., Convit, A., de Santi, S., and Bobinski, M. 1999. Structural neuroimaging: early diagnosis and staging of Alzheimer's disease. In *Alzheimer's Disease and Related Disorders* (K. Iqbal, B. Winblad, T. Nishimura, M. Takeda, and H. M. Wisniewski, Eds.), Vol. 14, pp. 105–126. Wiley, New York.

Desgranges, B., Baron, J. C., and Eustache, F. 1998a. The functional neuroanatomy of episodic memory: The role of the frontal lobes, the hippocampal formation and other areas. *NeuroImage* **8:** 198–213.

Desgranges, B., Baron, J. C., de La Sayette, V., Petit-Taboué, M. C., Lechevalier, B., and Eustache, F. 1998b. The neural substrates of memory systems in Alzheimer's disease: A PET study of resting brain glucose utilization. *Brain* **121:** 1158–1165.

Double, K. L., Halliday, G. M., Kril, J. J., Harasty, J. A., Cullen, K., Brooks, W. S., Creasey, H., and Broe, G. A.. 1996. Topography of brain atrophy during normal aging and Alzheimer's disease. *Neurobiol. Aging* **17:** 513–521.

Duyckaerts, C., Colle, M. A., Dessi, F., Grignon, Y., Piette, F., and Hauw, J. J. 1998. The progression of the lesions in Alzheimer's disease: Insights from a prospective clinicopathological study. *J. Neural Trans.* **53:** 119–126.

Erkinjuntti, T., Lee, D. H., Gao, F., Steenhuis, R., Eliasziw, M., Fry, R., Merskey, H., and Hachinski, V. C. 1993. Temporal lobe atrophy on magnetic resonance imaging in the diagnosis of early Alzheimer's disease. *Arch. Neurol.* **50:** 305–310.

Eustache, F., Desgranges, B., Aupée, A. M., Guillery, B., and Baron, J. C. 2000. The functional neuroanatomy of amnesia: Positron emission tomography studies. *Microsc. Res. Tech.* **51:** 94–100.

Fama, R., Sullivan, E. V., Shear, P. K., Marsh, L., Yesavage, J. A., Tinklenberg, J. R., Lim, K. O., and Pfefferbaum, A. 1997. Selective cortical and hippocampal volume correlates of Mattis dementia rating scale in Alzheimer's disease. *Arch. Neurol.* **54:** 719–728.

Foundas, A. L., Leonard, C. M., Mahoney, S. M., Agee, O. F., and Heilman, K. M. 1997. Atrophy of the hippocampus, parietal cortex, and insula in Alzheimer's disease: A volumetric magnetic resonance imaging study. *Neuropsychiatry Neuropsychol. Behav. Neurol.* **10:** 81–89.

Fox, N. C., Freeborough, P. A., and Rossor, M. N. 1996. Visualisation and quantification of rates of atrophy in Alzheimer's disease. *Lancet* **348:** 94–97.

Frisoni, G. B., Beltramello, A., Weiss, C., Geroldi, C., Bianchetti, A., and Trabucchi, M. 1996. Linear measures of atrophy in mild Alzheimer's disease. *AJNR* **17:** 913–923.

Frisoni, G. B., Laakso, M. P., Beltramello, A., Geroldi, C., Bianchetti, A., Soininen, H., and Trabucchi, M. 1999. Hippocampal and entorhinal cortex atrophy in frontotemporal dementia and Alzheimer's disease. *Neurology* **52:** 91–100.

Friston, K. J., Holmes, A. P., Worsley, K. J., Poline, J. B., Frith, C. D., and Frackowiak, R. S. J. 1995a. Statistical parametric maps in functional imaging: A general linear approach. *Hum. Brain Map.* **2:** 189–210.

Friston, K. J., Holmes, A., Poline, J. B., Price. C. J., and Frith, C. D. 1995b. Detecting activations in PET and fMRI: Levels of inference and power. *NeuroImage* **4:** 838–843.

Grignon, Y., Duyckaerts, C., Bennecib, M., and Hauw, J. J. 1998. Cytoarchitectonic alterations in the supramarginal gyrus of late-onset Alzheimer's disease. *Acta Neuropathol.* **95:** 395–406.

Haratounian, V., Purohit, D., Perl, D. P., Marin, D., Khan, K., Lantz, M., Davis, K. L., and Mohs, R. C. 1999. Neurofibrillary tangles in nondemented elderly subjects and mild Alzheimer disease. *Arch. Neurol.* **56:** 713–718.

Hasboun, D., Chantome, M., and Zouaoui, A., *et al.* 1996. MR determination of hippocampal volume: Comparison of three methods. *AJNR* **17:** 1091–1098.

Ibanez, V., Pietrini, P., Alexander, G. E., Furey, M. L., Teichberg, D., Rajapakse, J. C., Rapoport, S. I., Schapiro, M. B., and Horwitz, B. 1998. Regional glucose metabolic abnormalities are not the result of atrophy in Alzheimer's disease. *Neurology* **50:** 1585–1593.

Juottonen, K., Laakso, M. P., Insausti, M., Lehtovirta, M., Pitkanen, A., Partanen, K., and Soininen, H. 1998. Volumes of the entorhinal and perirhinal cortices in Alzheimer disease. *Neurobiol. Aging* **19:** 15–22.

Killiany, R. J., Gomez-Isla, T., Moss, M., Kikinis, R., Sandor, T., Jolesz, F., Tanzi, R., Jones, K., Hyman, B. T., and Albert, M. 2000. Use of structural magnetic resonance imaging to predict who will get Alzheimer's disease. *Ann. Neurol.* **47:** 430–439.

Larner, A. J. 1997. The cerebellum in Alzheimer's disease. *Dement. Geriatr. Cogn. Disord.* **8:** 203–209.

Lehéricy, S., Baulac, M., and Chiras, J., *et al.* 1994. Amygdalohippocampal MR volume measurements in the early stages of Alzheimer's disease. *Am. J. Neuroradiol.* **15:** 927–937.

Lowenstein, D. A., Barker, W. A., and Chang, J. Y., *et al.* 1989. Predominant left hemisphere metabolic dysfunction in dementia. *Arch. Neurol.* **46:** 146–152.

Maguire, E. A., Gadian, D. G., Johnsrude, I. S., Good, C. D., Ashburner, J., and Frackowiak, R. S. J., and Frith, C. D. 2000. Navigation-related structural change in the hippocampi of taxi drivers. *Proc. Natl. Acad. Sci. USA* **97:** 4398–4403.

Masliah, E., Terry, R. D., and Alford, M., *et al.* 1991. Cortical and subcortical patterns of synaptophysin-like immunoreactivity in Alzheimer's disease. *Am. J. Pathol.* **138:** 235–246.

Maunoury, C., Michot, J. L., Caillet, H., Parlato, V., Leroy-Willig, A., Jehenson, P., Syrota, A., and Boller, F. 1996. Specificity of temporal amygdala atrophy in Alzheimer's disease: Quantitative assessment with MRI. *Dementia* **7:** 10–14.

May, A., Ashburner, J., and Büchel, C., *et al.* 1999. Correlation between structural and functional changes in idiopathic headache syndrome. *Nature Med.* **5:** 836–838.

McKhann, G., Drachman, D., and Folstein, M., *et al.* 1984. Clinical diagnosis of Alzheimer's disease: Report of the NINCDS-ADRDA work group under the auspices of department of health and human services task force on Alzheimer's disease. *Neurology* **34:** 939–944.

Minoshima, S., Giordani, B., Berent, S., Frey, K. A., Foster, N. L., and Kuhl, D. E. 1997. Metabolic reduction in the posterior cingulate cortex in very early Alzheimer's disease. *Ann. Neurol.* **42:** 85–94.

Mummery, C. J., Patterson, K., Price, C. J., Ashburner, J., Frackowiak, R. S. J., and Hodjes, J. R. 2000. A voxel-based morphometry

study of semantic dementia: Relationship between temporal lobe atrophy and semantic memory. *Ann. Neurol.* **47:** 36–45.

Pantel, J., Schroder, J., Schad, L. R., Friedlinger, M., Knopp, M. V., Schmitt, R., Geissler, M., Bluml, S., Essig, M., and Sauer, H. 1997. Quantitative magnetic resonance imaging and neuropsychological functions in dementia of the Alzheimer type. *Psychol. Med.* **27:** 221–229.

Price, J. L., and Morris, J. C. 1999. Tangles and plaques in nondemented aging and 'preclinical' Alzheimer's disease. *Ann. Neurol.* **45:** 358–368.

Pruessner, J. C., Li, L. M., Serles, W., Pruessner, M., Collins, D. I., Kabani, N., Lupien, S., and Evans, A. C. 2000. Volumetry of hippocampus and amygdala with high-resolution MRI and three-dimensional analysis software: minimizing the discrepancies between laboratories. *Cereb. Cortex* **10:** 433–442.

Reiman, E. M., Caselli, R. J., Yun, L. S., Chen, K., Bandy, D., Minoshima, S., Thibodeau, S. N., and Osborne, D. 1996. Preclinical evidence of Alzheimer's disease in persons homozygous for the e4 allele for apolipoprotein E. *N. Engl. J. Med.* **334:** 752–758.

Richardson, M., Friston, K., and Sisodiya, S., *et al.* 1997. Cortical gray matter and benzodiazepine receptors in malformations of cortical development—A voxel-based comparison of structural and functional imaging data. *Brain* **120:** 1961–1973.

Rombouts, S. A., Barkhof, F., Witter, M. P., and Scheltens, P. 2000. Unbiased whole-brain analysis of gray matter loss in Alzheimer's disease. *Neurosci. Lett.* **19:** 231–233.

Small, G. W., Ercoli, L. M., and Siverman, D. H. S., *et al.* 2000. Cerebral metabolic and cognitive decline in persons at genetic risk for Alzheimer's disease. *Proc. Natl. Acad. Sci. USA* **97:** 6037–6042.

Smith, A. D., and Jobst, K. A. 1996. Use of structural imaging to study the progression of Alzheimer's disease. *Br. Med. Bull.* **52:** 575–586.

Talairach, J., and Tournoux, P. 1988. *Co-planar Stereotaxic Atlas of the Human Brain—3-Dimensional Proportional System: An Approach to Cerebral Imaging.* Thieme, New York.

Van Hoesen, G. W., Parvizi, J., and Chu, C. C. 2000. Orbitofrontal cortex pathology in Alzheimer's disease. *Cereb. Cortex* **10:** 243–251.

Vogt, B. A., Vogt, L. J., Vrana, K. E., Gioia, L., Meadows, R. S., Challa, V. R., Hof, P. R., and Van Hoesen, G. W. 1998. Multivariate analysis of laminar patterns of neurodegeneration in posterior cingulate cortex in Alzheimer's disease. *Exp. Neurol.* **153:** 8–22.

Worsley, K. J., Marrett, S., Neelin, P., Vandal, A. C., Friston, K., and Evans, A. C. 1996. A unified statistical approach for determining significant voxels in images of cerebral activation. *Hum. Brain Map.* **8:** 98–101.

Wright, J., McGuire, P., and Poline, J. B., *et al.* 1995. A voxel-based method for the statistical analysis of grey and white matter density applied to schizophrenia. *NeuroImage* **2:** 244–252.

Xu, Y., Jack, C. R., and O'Brien, P. C., *et al.* 2000. Usefulness of MRI measures of entorhinal cortex versus hippocampus in AD. *Neurology* **54:** 1760–1767.